Upconversion Properties of Ln^{3+} Doped $NaYF_4$/Polymer Composite Fibers Prepared by Electrospinning

Biao Dong,[†] Hongwei Song,*[,‡] Hongquan Yu,[†] Hui Zhang,[†] Ruifei Qin,[†] Xue Bai,[†] Guohui Pan,[†] Shaozhe Lu,[†] Fang Wang,[†] Libo Fan,[†] and Qilin Dai[†]

Key Laboratory of Excited State Physics Changchun Institute of Optics, Fine Mechanics and Physics Chinese Academy of Sciences, and Graduate School of Chinese Academy of Sciences, 16 Eastern South-Lake Road, Changchun 130033, P. R. China, and College of Electronic Science and Engineering, JiLin University, ChangChun 130012, P. R. China

Received: August 30, 2007; In Final Form: October 31, 2007

Ln^{3+} doped (Yb^{3+},Tm^{3+} codoped and Yb^{3+},Er^{3+},Tm^{3+} tridoped) $NaYF_4$/poly(vinyl pyrrolidone)(PVP) ($M_w \approx 1\,300\,000$) composite fibers with an average diameter of 300−800 nm were prepared by electrospinning and characterized by X-ray diffraction, field emission scanning electron micrography, and Fourier transform infrared spectra. Their upconversion (UC) luminescence properties were studied in contrast to the corresponding Ln^{3+} doped $NaYF_4$ nanoparticles (15−20 nm) under 980-nm excitation. The results demonstrate that in the Yb^{3+},Tm^{3+} codoped composite fibers the blue emission of $^1G_4$-$^3H_6$ is dominantly strong, while in the nanoparticles the red emission of $^3F_{2,3}$-$^3H_6$ contributes considerably to the increase of the excitation power. This indicates that the color purity of blue is improved greatly by the modification of PVP. In the tridoped Yb^{3+},Er^{3+},Tm^{3+} composite fibers, white light with more stable color balance (blue $^1G_4$-$^3H_6$ of Tm^{3+}, green $^2H_{11/2}$/$^4S_{3/2}$-$^4I_{15/2}$, and red $^4F_{9/2}$-$^4I_{15/2}$ of Er^{3+}) was obtained. The improved UC properties in the composite fibers are attributed to the suppressed local thermal effect. The energy transfer and UC populating processes are discussed.

I. Introduction

In recent years, much attention has been paid to nanostructures with controllable sizes, shapes, and compositions.[1] For a broad range of applications, one-dimensional (1D) nanostructures are of fundamental importance.[2−4] These complex architectures, such as nanowires, nanorods, nanobelts, and nanotubes, are expected to display an important role for both fundamental studies and technological applications.[5−7]

A large number of synthetic and fabrication methods have already been demonstrated for generating 1D nanostructures, such as using an anodic aluminum oxide template,[8] homogeneous precipitation,[9] hydrothermal or solvothermal treatment,[10−12] and so on. These methods are usually employed to produce inorganic 1D nanostructures; however, they are incapable of preparing 1D organic−inorganic nanomaterials.

Electrostatic fiber formation, so-called electrospinning, is a simple, convenient, and versatile technique for generating long fibers with diameters ranging from tens of nanometers up to micrometers. It has been demonstrated that a variety of materials, such as organic,[13−15] inorganic,[16−18] and hybrid polymers (organic−inorganic composites)[19,20] can be electrospun to form uniform fibers.[21] These systems that combine both inorganic and organic characters are found to have the advantage in many fields of application, such as membrane technology,[22] tissue engineering,[23] optical sensors, biosensors,[24] superhydrophobic surfaces,[23] and drug delivery.[25]

In this paper, we demonstrate the experimental studies on lanthanide doped $NaYF_4$/PVP composite fibers in contrast to $NaYF_4$ nanoparticles. It is well known that $NaYF_4$ is a superior material, and many works have been done to study the structure and UC mechanism.[26−29] In particular, Yb^{3+},Tm^{3+} and Yb^{3+},Er^{3+} codoped $NaYF_4$ nanocrystals are known as some of the most efficient UC materials because of the very low phonon energies of their lattices.[30−34] However, the organic modified UC materials have not been reported, to our knowledge. PVP is an important organic material in optical and electric design. It is expected that the existence of PVP not only can control the structural properties in electrospining but also can modify the UC luminescence processes of rare earth ions.

In the present work, $NaYF_4$:Yb^{3+},Tm^{3+}/PVP composite fibers were investigated and it was observed that the energy transfer and UC luminescence processes of $NaYF_4$: Yb^{3+},Tm^{3+} nanocrystals in the composite fibers were modified greatly because of the interaction between PVP and Tm^{3+}. Furthermore, white light was designed and generated by doping another lanthanide ion, Er^{3+} (red and green), into the $NaYF_4$:Yb^{3+},Tm^{3+}(blue) system under the excitation of a 980-nm laser diode. More stable white light was observed in the composite fibers in comparison to the nanoparticles. To the best of our knowledge, there was no study on the modification of PVP to lanthanide ions, which makes it of particular interest as a lighting material with great application potential.

II. Experimental Section

In a typical experiment, $NaYF_4$/PVP composite fibers were prepared by electrospinning from a solution containing $NaYF_4$ nanoparticles and PVP with different ratios. The schematic

* Corresponding author. E-mail: hwsong2005@yahoo.com.cn. Fax: 86-431-86176320.

† Key Laboratory of Excited State Physics Changchun Institute of Optics, Fine Mechanics and Physics Chinese Academy of Sciences, and Graduate School of Chinese Academy of Sciences.

‡ JiLin University.

10.1021/jp076958z CCC: $40.75
Published on Web 01/16/2008

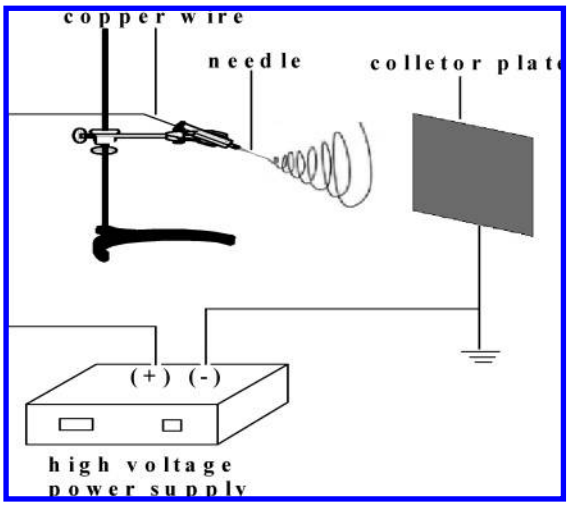

Figure 1. Schematic diagram of the electrospinning setup.

diagram of the electrospinning setup was shown in Figure 1.[35] It consisted of three major components: a high-voltage power supply, a spinneret (a needle), and a collector plate (a grounded conductor). As a nonmechanical fiber drawing method, electrospinning involved the stretching of inorganic nanomaterials and polymer hybrid solution (or melt) with electrostatic forces. The voltage used for electrospinning was 13 kV.

For the synthesis of the lanthanide doped $NaYF_4$ colloids, polyol method was employed in this work. In the preparation of $NaYF_4$:Yb^{3+},Tm^{3+} nanoparticles, stoichiometric amounts of NaF (99.99%), $Y(NO_3)_3{\cdot}6H_2O$, $Yb(NO_3)_3{\cdot}6H_2O$, $Tm(NO_3)_3{\cdot}6H_2O$ were mixed together with a desirable amount of diethylene glycol (DEG, 98%, A. R.) to make the metal ion concentration 0.02 mol/L and then transferred to a round-bottomed flask. The mixture was heated to 180 °C in a silicon oil bath under vigorous stirring for 2 h. When the suspension was cooled to room temperature, the colloids were separated by centrifugation and washed with ethanol several times. The preparation procedure of $NaYF_4$:Yb^{3+},Er^{3+},Tm^{3+} nanoparticles was same as that of $NaYF_4$:Yb^{3+},Tm^{3+} nanoparticles.

It is well known that the homogenization of the composite fibers is one of the most important factors of its optical and mechanical properties. Note that the aggregation of nanoparticles always happens in the drying and annealing process. So, in this work we avoided the nanoparticle drying step and added an appropriate amount of PVP directly to $NaYF_4$ colloids according to the weight ratio of PVP to $NaYF_4$ colloids of 1:1, 2:1, 3:1, and 4:1. A long time of stirring and ultrasonic was then carried out to obtain a homogeneous hybrid solution. Successful electrospinning requires the use of an appropriate solvent and hybrid-polymer system to prepare solutions exhibiting the desired viscoelastic behavior. The viscous solution of $NaYF_4$/PVP composites was controlled by adding enough ethanol to make the weight ratio of PVP to ethanol 12 wt %. After stirring, the final solution was then electrospun to form composite fibers.

The X-ray diffraction (XRD) data of the fibers was collected on Rigaku D/max-rA X-ray diffractometer using a Cu target radiation source. The morphology of the fibers was inspected using a Hitachi S-4800 field emission scanning electron micrograph (FE-SEM). Fourier transform infrared spectroscopy (FTIR) was recorded in the range of 700−4000 cm^{-1} on a Fourier transform spectrometer (Perkin-Elmer, Spectrum 1) with a resolution of 1 cm^{-1}. The emission spectra were recorded at room temperature using a Hitachi F-4500 fluorescence spectrometer equipped with a 980-nm laser diode. UC fluorescence

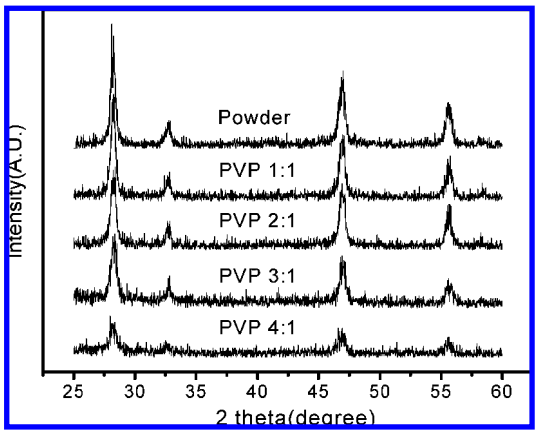

Figure 2. XRD patterns of the of $NaYF_4$ nanoparticles and composite fibers.

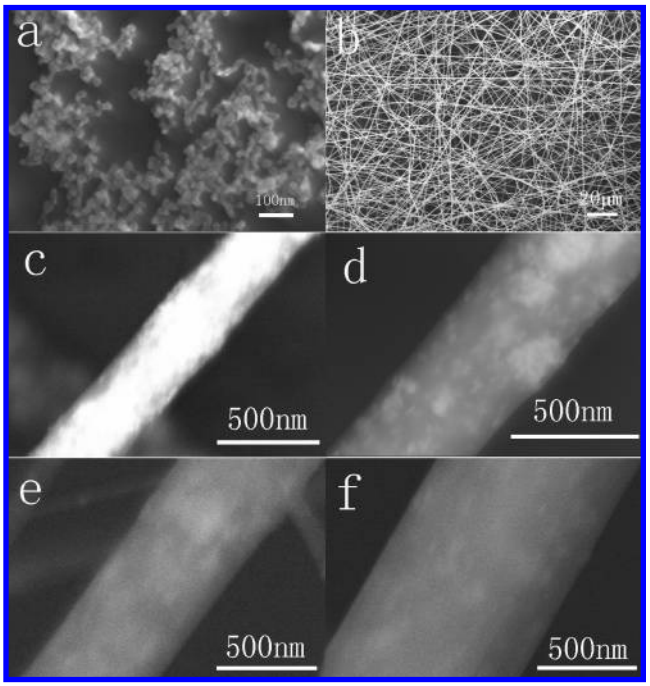

Figure 3. SEM images of the nanoparticles and the fibers. (a) Nanoparticles. (b) General view of the fibers. (c−f) Magnified SEM images of the composite fibers with ratios of 1:1 to 1:4.

dynamics were measured under the excitation of a 980-nm optical parameter oscillator (OPO) laser pumped by a pulsed Nd:YAG laser, which had a pulse duration of 10 nm and a repetition frequency of 10 Hz.

III. Results and Discussion

A. Structure and Morphology. Figure 2 shows the XRD patterns of $NaYF_4$ nanoparticles and the composite fibers with different ratios of PVP to $NaYF_4$. The powder sample was well-crystallized, and all of the peaks could be readily indexed to the cubic $NaYF_4$ phase. Also, peaks of the cubic $NaYF_4$ phase appeared in all of the composite fiber samples, implying the existence of $NaYF_4$ nanoparticles in the composite fibers.

Figure 3 depicts SEM images of the samples. Figure 3a shows that the $NaYF_4$ nanoparticles are dispersed uniformly and the average size of them is 15−20 nm. The general overview SEM image in Figure 3b shows that the fibers are oriented randomly and the lengths of them are several 10 mm. Figure 3c−f shows the enlarged images of single fibers of the samples with ratios of 1:1 to 4:1. The diameters of the samples are ∼300, 400, 500,

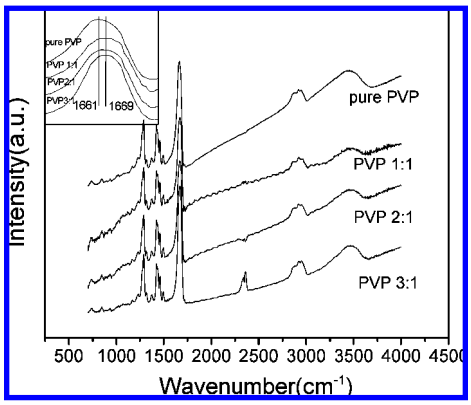

Figure 4. Infrared absorption spectra of the pure PVP and the composite fibers; the inset is the magnified absorption peak of C═O.

and 800 nm, respectively, corresponding to the 1:1, 2:1, 3:1, and 4:1 samples. In the sample with a ratio of 1:1, it can be seen that some nanoparticles aggregate together. As for the other samples, the $NaYF_4$ nanoparticles are dispersed homogeneously in the composite fibers.

Figure 4 shows the FTIR of pure PVP and composite fibers. The FTIR spectra of the composite fibers were similar to that of the pure PVP fiber in the studied range. A broad band at 3400 cm^{-1} was observed in the pure and composite fibers, which was generated by vibrations of associated hydroxyl groups. The contamination of trace hydroxyl groups in the fibers was due to the electrospun solution. The absorption peak of the C═O group in the PVP located at 1660 cm^{-1}, whereas in the composite fibers it shifted to 1669 cm^{-1} (see the inset of Figure 4), which indicated that $NaYF_4$ nanoparticles were stabilized through chemical interactions with the oxygen atoms of the polypyrrolidone units of PVP. This interaction might come from the donation of a pair of electron transfers from the carbonyl oxygen to lanthanide ions.

B. UC Luminescence of $NaYF_4$:Yb^{3+},Tm^{3+}/PVP Composite Fibers. Figure 5a shows the normalized UC luminescence spectra in the $NaYF_4$:Yb^{3+},Tm^{3+} nanoparticles under different excitation powers. The blue emission centers at ~476 nm, corresponding to the $^1G_4$-$^3H_6$ transition of Tm^{3+}. A weak shoulder corresponding to the $^1D_2$-$^3F_4$ transition appears at 451 nm. The emission at 649 nm corresponds to the transition of $^1G_4$-$^3F_4$ of Tm^{3+}. The emissions from 660 to 740 nm are attributed to $^3F_{2,3}$-$^3H_6$ transitions of Tm^{3+}, as labeled in the figure. Because the excitation power is lower, the $^1G_4$-$^3H_6$ blue emission is dominantly strong. As the excitation power increases to 1450 mW, the $^3F_{2,3}$-$^3H_6$ red emissions increase more intensively relative to the blue and the sample displays mixed color of blue and red. In addition, it can be also observed that the intensity ratio of $^3F_2$-$^3H_6$ to $^3F_3$-$^3H_6$ varies greatly with the increase of excitation power. This intensity ratio as a function of excitation power is drawn as Figure 9a. The ratio increases originally with excitation power, then approaches at a maximum, and then decreases with excitation power. The origin of the intensity ratio variation is caused by the thermal effect caused by laser irradiation, which will be discussed later. A similar result was also observed and discussed in Y_2O_3:Er^{3+},Yb^{3+} nanocrystals.[36]

Figure 5b depicts the normalized UC luminescence spectra in the 1:1 composite fibers. It can be seen that as the excitation power varies the $^1G_4$-$^3F_4$ blue emission is dominant all the time, which differs from the nanoparticles. In addition, because the excitation power is high enough, the blue emission at 451 nm originating from the $^1D_2$-$^3F_4$ transition becomes stronger and

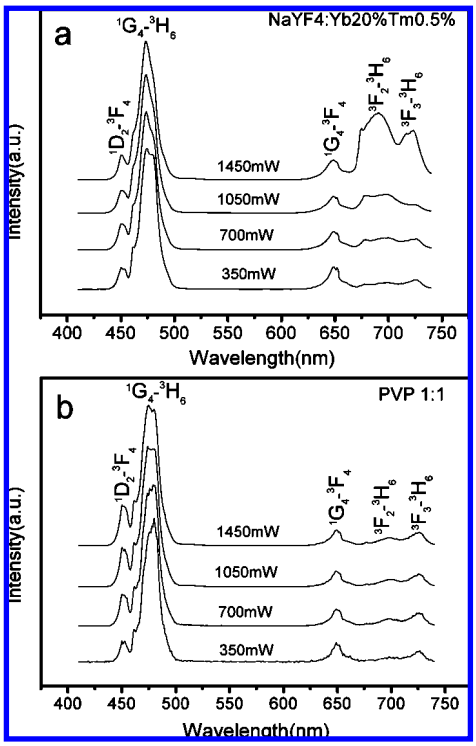

Figure 5. Normalized UC spectra of the (a) $NaYF_4$:Yb^{3+}(20%),Tm^{3+}-(0.5%) nanoparticles and (b) composite fibers with ratios of 1:1.

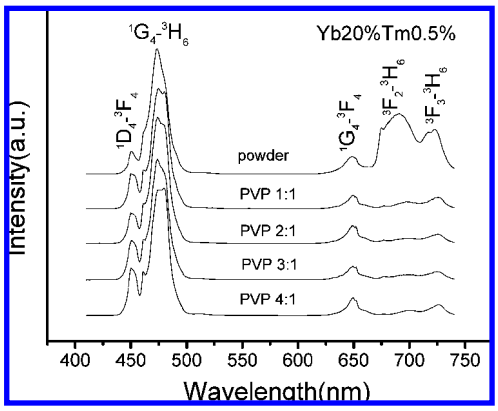

Figure 6. Energy level diagrams of the Yb^{3+}, Tm^{3+} ions and UC mechanisms following excitation with 980 nm. The full, dotted arrows represent emission, energy transfer, and multiphonon relaxation processes.

the red emissions from 660 to 740 nm become weaker in comparison to the nanoparticles. The intensity ratio of $^3F_2$ -$^3H_6$ to $^3F_3$ -$^3H_6$ in the composite fibers has only a little variation in contrast to that in the pure nanoparticles (see Figure 9a).

Figure 6 shows the normalized UC emission spectra of the nanoparticles and the composite fibers with different concentrations of PVP. It is obvious that the intensity of $^1D_2$-$^3F_4$ relative to $^1G_4$-$^3H_6$ increases gradually with the increase of PVP concentration. As the PVP concentration varies, the intensity of $^3F_{2,3}$-$^3H_6$ relative to $^1G_4$-$^3H_6$ has little variation.

C. Energy Transfer and UC Luminescence Processes of $NaYF_4$:Yb^{3+},Tm^{3+}. To better understand the UC mechanism in $NaYF_4$:Yb^{3+},Tm^{3+}, the energy transfer and UC luminescence processes under 980-nm excitation are drawn as Figure 7.[37] First, the electrons on ground states $^3H_6$ are excited to $^3H_5$ through the fist-step energy transfer of Yb^{3+} → Tm^{3+} and then the electrons on $^3H_5$ relax to $^3F_4$. Second, the electrons on $^3F_4$ are excited to $^3F_2$ through the second-step energy transfer, which

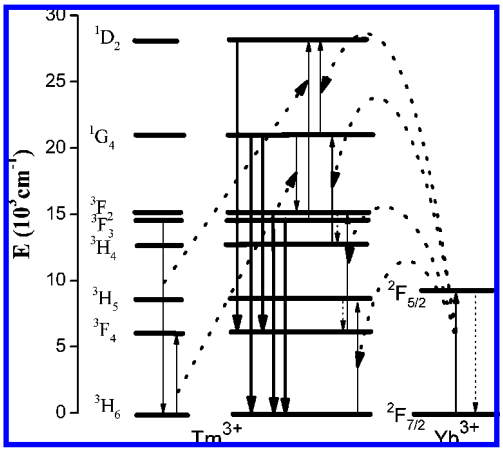

Figure 7. Normalized UC spectra at a pump power of 1450 mW in $NaYF_4:Yb^{3+},Tm^{3+}$ nanoparticles and $NaYF_4:Yb^{3+},Tm^{3+}$/PVP composite fibers.

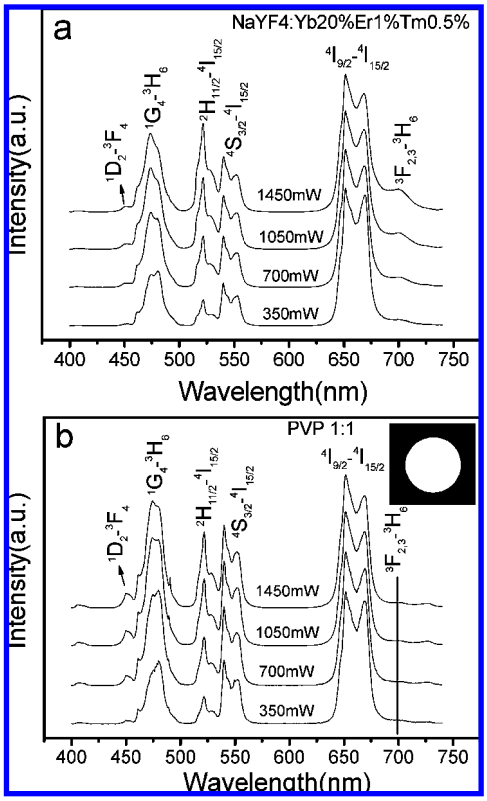

Figure 8. Normalized UC spectra at various pump powers in (a) $NaYF_4:Yb^{3+},Er^{3+},Tm^{3+}$ nanoparticles and (b) composite fibers with ratios of 1:1. The inset: the luminescence spot on the fiber sample with an excitation power of 1450 mW.

can generate red emission of $^3F_{2,3}$-$^3H_6$ or relax to $^3H_4$. Third, the electrons on $^3H_4$ are excited to $^1G_4$ through the third-step energy transfer, generating blue $^1G_4$-$^3H_6$ or red $^1G_4$-$^3F_4$ emission.[38] The electrons on $^1G_4$ could also be excited to $^1D_2$ through the fourth-step energy transfer, generating blue $^1D_2$-$^3F_4$ emission.

In the $NaYF_4:Yb^{3+},Tm^{3+}$ system, because the doping concentration of Tm^{3+} is as high as 0.5%, the following cross relaxation processes probably happen because the excitation power is high enough, as marked in Figure 7:

$$Tm(A)^1G_4 + Tm(B)^3H_6 \rightarrow Tm\ (A)^3F_{2,3} + Tm(B)^3F_4 \quad (1)$$

$$Tm(A)\ ^3F_3 + Tm(B)\ ^3F_3 \rightarrow Tm(A)^1D_2 + Tm(B)\ ^3H_6 \quad (2)$$

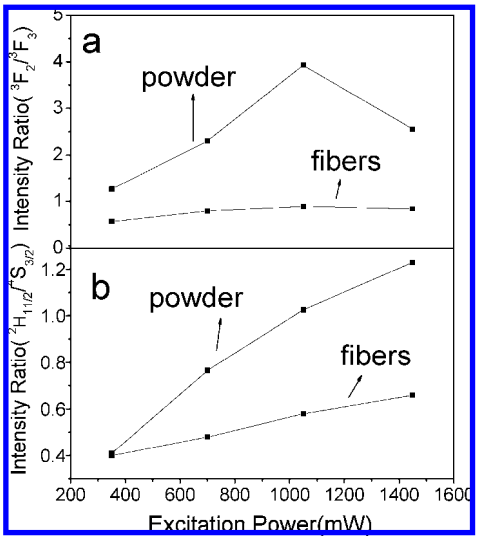

Figure 9. Dependence of the intensity ratio of $^3F_2$-$^3H_6$/$^3F_3$-$^3H_6$(Tm^{3+}) (a) and $^2H_{11/2}$-$^4I_{15/2}$/$^4S_{3/2}$-$^4I_{15/2}$(Er^{3+}) (b) of the nanoparticles and the composite fibers on the excitation power.

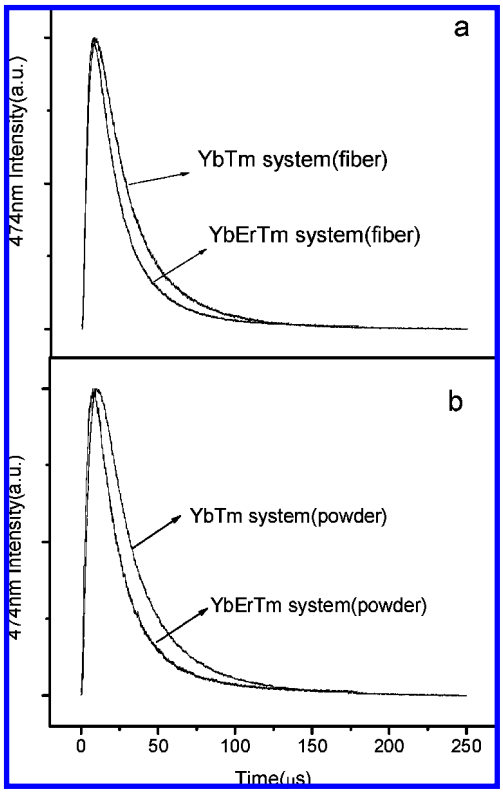

Figure 10. Luminescence decay curves of $^1G_4$-$^3H_6$ transitions at 474 nm in (Yb^{3+}, Tm^{3+}) codoped and (Yb^{3+}, Er^{3+}, Tm^{3+}) tridoped $NaYF_4$ nanoparticles and $NaYF_4$/PVP composite fibers.

In the nanoparticles, because the excitation power is high enough, the local thermal effect caused by laser irradiation is evident, which leads the temperature at the irradiated spot to increase largely.[12] This can be concluded from the fact that the intensity ratio of $^3F_2$-$^3H_6$ to $^3F_3$-$^3H_6$ varies greatly with the increase of excitation power. The energy gap between $^3F_2$ and $^3F_3$ states is only about 500 cm^{-1}. The population distribution between the two states is dominated by Bolzmann's distribution, and thus the intensity ratio is a critical parameter in detecting the local temperature. The increased local temperature leads the population of $^3F_3$ to decrease considerably because of thermal activation, while the population of $^3F_2$ relative to $^3F_3$ increases.

TABLE 1: Rise and Decay Time Constants of Er^{3+} and Tm^{3+} in the Presence and Absence of PVP

energy levels		474 nm ($^1G_4$-$^3H_6$)	550 nm ($^4S_{3/2}$-$^4I_{15/2}$)	650 nm ($^4F_{9/2}$-$^4I_{15/2}$)	energy levels		474 nm ($^1G_4$-$^3H_6$)
Yb^{3+},Er^{3+},Tm^{3+}	$\tau_1(\mu s)$	41	17	9	Yb^{3+},Tm^{3+}	$\tau_1(\mu s)$	61
nanoparicles	$\tau_2(\mu s)$	199	126	44	nanoparicles	$\tau_2(\mu s)$	250
Yb^{3+},Er^{3+},Tm^{3+}	$\tau_1(\mu s)$	40	16	9	Yb^{3+},Tm^{3+}	$\tau_1(\mu s)$	48
fibers	$\tau_2(\mu s)$	186	118	43	fibers	$\tau_2(\mu s)$	236

As a consequence, the cross relaxation process (2) is not effective. However, the cross relaxation process (1) is effective in the nanoparticles, which leads to the population increase of $^3F_2$ relative to the $^1G_4$ and the intensity increase of $^3F_2$-$^3H_6$ relative to $^1G_4$ -$^3H_6$.

The emission changes for the composite fibers can be attributed to the interaction between the $NaYF_4$:Yb^{3+},Tm^{3+} nanoparticles and PVP. Some vibration transitions of the PVP may match the energy separations between the two neighboring excited levels exactly and change the populating channels through efficient nonradiative energy transfer. For example, the vibrational absorption of C═O peaking at 1660 cm^{-1} matches the energy separation between the red level $^3F_2$ and the neighboring downlevel $^3H_4$ ($\sim$ 1680 cm^{-1}) of Tm^{3+} exactly; thus, it is suggested that the carbonyl group bridges the nonradiative relaxation of $^3F_2$-$^3H_4$ of Tm^{3+} effectively. The depopulation on $^3F_2$ leads to the emission decrease of $^3F_2$-$^3H_6$. At the same time, the improved population on $^3H_4$ causes the energy transfer of $^3H_4(Tm^{3+}) + {}^2F_{7/2}(Yb^{3+}) \rightarrow {}^1G_4(Tm^{3+}) + {}^2F_{5/2}(Yb^{3+})$ to happen effectively.

The effective thermal exchange between Tm^{3+} ions and PVP also induces the temperature surrounding Tm^{3+} to have only a slight increase in contrast to that in the pure nanoparticles. Thus, a large number of electrons still distribute on the $^3F_3$ state after two-step energy transfers. The cross relaxation process (2) happens effectively, resulting in the intensity increase of $^1D_2$-$^3H_6$ relative to $^1G_4$-$^3H_6$.[31]

D. $NaYF_4$:Yb^{3+}, Er^{3+},Tm^{3+} White Light-Emitting Fibers. For a variety of purposes, generation of efficient and stable UC white light sources is important.[39] UC white light-emitting fibers with simultaneous blue, green, and red emissions were designed and generated in the $NaYF_4$:Yb^{3+},Er^{3+},Tm^{3+} composite fibers. Tricolor emissions were generated by Er^{3+} (red and green) and Tm^{3+}(blue). Codoping of Yb^{3+} can greatly increase the sensitivity of photoluminescence of Er^{3+} and Tm^{3+} through energy transfer because of its efficient absorption at 980 nm. Controlling the doping content of the lanthanide ions is significant for the color balance of white light. In $NaYF_4$ nanoparticles, as the concentrations of Er^{3+}, Tm^{3+}, Yb^{3+} were adjusted, respectively, to be 1.0, 0.5, and 20% in molar ratio, bright white emission was obtained.

Figure 8a shows the normalized spectra of the $NaYF_4$:Yb^{3+},-Er^{3+},Tm^{3+} nanoparticles under excitation with different powers. It can be seen that all of the tricolor emission lines appear in the visible range. Besides the blue emissions centered at $\sim$478 nm of Tm^{3+}, the green emissions of $^2H_{11/2}$/$^4S_{3/2}$-$^4I_{15/2}$ of Er^{3+} also appear. The peaks in the red region of 641−725 nm correspond to the stronger $^4F_{9/2}$-$^4I_{15/2}$ transition of Er^{3+} as well as weaker $^3F_{2,3}$-$^3H_6$ transition of Tm^{3+}, as labeled in the figure. Note that in the tridoped system as the excitation power varied, a similar tendency for the $^3F_{2,3}$-$^3H_6$ transition of Tm^{3+} was observed, like that in the $NaYF_4$: Yb^{3+},Tm^{3+} codoped system. In addition, when the excitation power increases, the intensity ratio of $^2H_{11/2}$-$^4I_{15/2}$ to $^4S_{3/2}$-$^4I_{15/2}$ also increases, which can also be attributed to local thermal effect induced by the exposure of the laser diode.[9] In the nanoparticles, the white color balance changes unexpectedly with excitation power because of the variation of the intensity ratio of the green $^2H_{11/2}$/$^4S_{3/2}$-$^4I_{15/2}$ (Er^{3+}) to the blue $^1G_4$-$^3H_6$ (Tm^{3+}) as well as the red $^4F_{9/2}$-$^4I_{15/2}$ (Er^{3+}).

Normalized UC spectra in the composite fibers with ratio of 1:1 at various pump powers are shown in Figure 8b. It can be seen that the intensity ratio of $^2H_{11/2}$-$^4I_{15/2}$ to $^4S_{3/2}$-$^4I_{15/2}$ had only a little variation, implying that the temperature at the irradiated spot changed a little.[9] The relative intensity for the emissions in different visible regions, blue, green, and red, had smaller a variation with excitation power, implying that the color balance is more stable as the excitation power varies. The luminescence spot on the sample with a ratio of 1:1 is inserted in Figure 8b.

The dependence of the intensity ratio of $^2H_{11/2}$-$^4I_{15/2}$ to $^4S_{3/2}$-$^4I_{15/2}$ of the nanoparticles and the composite fibers on the excitation power is plotted in Figure 9b. It can be seen that the intensity ratio increases with the excitation power for both samples. In the nanoparticles the intensity increases significantly, whereas in the composite fibers it increases slightly. The energy separation between $^2H_{11/2}$ and $^4S_{3/2}$ is $\sim$730 cm^{-1}. The population distribution between them is dominated by thermal activation, which depends strongly on temperature, similar to the $^3F_3$ and $^3F_2$ states of Tm^{3+}. The result in Figure 9 again indicates that in the tridoped composite fibers the thermal effect caused by laser exposure at the irradiated spot was suppressed, which was attributed to the modification of PVP in the composite fibers. The distorted vibration absorption of C−H peaking at 734 cm^{-1} matches the energy separation between the two green levels of Er^{3+}, $^2H_{11/2}$, and $^4S_{3/2}$ exactly, bridging the nonradiative relaxation of $^2H_{11/2}$-$^4S_{3/2}$ through nonradiative energy transfer from Er^{3+} to PVP and quenching the $^2H_{11/2}$-$^4I_{15/2}$ transitions. It is the energy transfer between Er^{3+} and PVP in the composite fibers that suppressed the thermal effect.

E. Upconversion Luminescent Dynamics. Dynamics of Yb^{3+},Tm^{3+}-codoped and Yb^{3+},Er^{3+},Tm^{3+}-tridoped systems with the presence and absence of PVP were measured and compared, as shown in Figure 10 ($^1G_4$-$^3H_6$ transition at 474 nm). It should be noted that the output power of the OPO pulsed laser (250 mW) is much lower than that of near-infrared laser diodes ($\geq$360 mW) and the lifetimes obtained from OPO only reflect the dynamics at low excitation power. It can be observed that the dynamics contains a faster rise process and a slower decay process. The rise process corresponds to the energy-transfer-induced population increase as the laser pulse is terminated originally, which depends strongly on the energy transfer rate. The luminescent dynamics are fitted with a universal function

$$I(t) = I_0(e^{-t/\tau_2} - e^{-t/\tau_1}) \quad (1)$$

where τ_1 and τ_2 are the rise and decay time constants, respectively. τ_1 depends mainly on the energy transfer rate from Yb^{3+} to Tm^{3+} or Er^{3+}, whereas τ_2 depends on the electronic transition rate of the related excited level. The luminescent dynamics of the other transitions were also measured, and the deduced rise and decay time constants were listed in Table 1. The results in Table 1 can be concluded as follows: (1) The

rise and decay time constants in the composite fibers have only a little variation in comparison to those in the pure nanoparticles, indicating that because the excitation power is lower the energy transfer rate from Yb^{3+} to Tm^{3+} (Er^{3+}) and the electronic transition rate of the related excited levels rarely vary. This implies that the UC efficiency in the composite fibers should also have little variation relative to the nanoparticles. (2) In the tridoped systems, the rise and decay time constants of the $^1G_4$-$^3H_6$ transition become shorter compared to those in the codoped systems. The decrease of the rise and decay time constants in the tridoped system is ascribed to the energy transfer process of $^1G_4(Tm^{3+}) + {}^4I_{15/2}(Er^{3+}) \rightarrow {}^3F_4(Tm^{3+}) + {}^4F_{9/2}(Er^{3+})$. The energy of the $^1G_4$-$^3F_4$ emission matches the excitation of $^4I_{15/2}$-$^4F_{9/2}$ exactly.

IV. Conclusions

Structural and UC luminescence properties of Ln^{3+} doped $NaYF_4$/PVP composite fibers prepared by electrospinning were studied in contrast to the corresponding Ln^{3+} doped $NaYF_4$ nanoparticles under 980-nm excitation. It is interesting to observe that the properties of UC luminescence are improved in the composite fibers. In the $NaYF_4$: Yb^{3+},Tm^{3+}/PVP composite fibers, the blue emission of $^1G_4$-$^3H_6$ is dominantly strong all the time, whereas in the nanoparticles the red emission of $^3F_{2,3}$-$^3H_6$ contributes considerably because the excitation power is high, indicating that the color purity of blue is improved greatly by the modification of PVP. In addition, the intensity ratio of $^3F_2$-$^3H_6$ to $^3F_3$-$^3H_6$ increases greatly with the increasing excitation power in the nanoparticles, while that has only a little increase in the composite fibers. This strongly suggests that the local temperature surrounding Tm^{3+} in the nanoparticles increased more in contrast to that in the fibers due to laser exposure. In other words, the thermal effect in the composite fibers is suppressed. As a consequence, the populating processes including cross relaxation processes varied greatly in different samples, which are described in detail in the text.

In the tridoped $NaYF_4$:Yb^{3+},Er^{3+},Tm^{3+}/PVP composite fibers, white light emission was generated by optimum concentrations of Tm^{3+}, Er^{3+}, and Yb^{3+}. More stable color balance (blue $^1G_4$-$^3H_6$ of Tm^{3+}, green $^2H_{11/2}$/$^4S_{3/2}$-$^4I_{15/2}$, and red $^4F_{9/2}$-$^4I_{15/2}$ of Er^{3+}) was obtained. The studies on UC dynamics suggests that in the composite fibers, because the excitation power was low, the electronic transition rate, the energy transfer rate, and the luminescence quantum yield had only a little variation in comparison to the nanoparticles. In conclusion, this kind of novel inorganic−organic UC composite has desirable UC properties, which is important for applications in lighting and display.

Acknowledgment. We are thankful for financial support by National Natural Science Foundation of China (Grant No. 10704073, 50772042 and 10504030) and the 863 Project of China (2007AA03Z314).

References and Notes

(1) Lauhon, L. J.; Gudiksen, M. S.; Wang, D.; Lieber, C. M. *Nature* **2002**, *420*, 57.

(2) Yang, P. D.; Yan, H. Q.; Mao, S.; Russo, R.; Johnson, J.; Saykally, R.; Morris, N.; Pham, J.; He, R. R.; Choi, H.-J. *Adv. Funct. Mater.* **2000**, *12*, 323.

(3) Wu, Y. Y.; Yan, H. Q.; Huang, M.; Messer, B.; Song, J. H.; Yang, P. D. *Chem.—Eur. J.* **2002**, *8*, 1260.

(4) Hu, J.; Odom, T. W.; Lieber, C. M. *Acc. Chem. Res.* **1999**, *32*, 435.

(5) Hu, J.; Ouyang, M. Y.; Lieber, C. M. *Nature* **1999**, *399*, 48.

(6) Xu, D. S.; Guo, G. L.; Gui, L. L.; Tang, Y. Q.; Shi, E. J.; Jin, E. X. *Appl. Phys. Lett.* **1999**, *75*, 481.

(7) Heath, J. R.; Kuekes, P. J.; Snyderg; Williams, R. S. *Science* **1998**, *280*, 717.

(8) Zhang, J.; Hong, G. *J. Solid State Chem.* **2004**, *177*, 1292.

(9) Wu, C. F.; Qin, W. P.; Qin, G. S.; Zhao, D.; Zhang, J. S.; Huang, S. H.; Lu, S. Z.; Liu, H. Q.; Lin, H. Y. *Appl. Phys. Lett.* **2003**, *82*, 520.

(10) He, Y.; Tian, Y.; Zhu, Y. F. *Chem. Lett.* **2003**, *32*, 862.

(11) Song, H.; Yu, L.; Lu, S.; Wang, T.; Liu, Z.; Yang, L. *Appl. Phys. Lett.* **2004**, *85*, 470.

(12) Lei, Y.; Song, H.; Yang, L.; Yu, L.; Liu, Z.; Pan, G.; Bai, X.; Fan, L. *J. Chem. Phys.* **2005**, *123*, 174710.

(13) Bognitzki, M.; Czado, W.; Frese, T.; Schaper, A.; Hellwig, M.; Steinhart, M.; Greiner, A.; Wendorff, J. H. *Adv. Mater.* **2001**, *13*, 70.

(14) Madhugiri, S.; Dalton, A.; Gutierrez, J.; Ferraris, J. P.; Balkus, K. J., Jr. *J. Am. Chem. Soc.* **2003**, *125*, 14531.

(15) Yao, L.; Haas, T. W.; Guiseppi-Elie, A.; Bowlin, G. L.; Simpson, D. G.; Wnek, G. E. *Chem. Mater.* **2003**, *15*, 1860.

(16) Li, D.; Xia, Y. *Nano Lett.* **2003**, *3*, 555.

(17) Larsen, G.; Velarde-Ortiz, R.; Minchow, K.; Barrero, A.; Loscertales, I. G. *J. Am. Chem. Soc.* **2003**, *125*, 1154.

(18) Ko, F.; Gogotsi, Y.; Ali, A.; Naguib, N.; Ye, H.; Yang, G.; Li, C.; Wills, P. *Adv. Mater.* **2003**, *15*, 1161.

(19) Ge, J. J.; Hou, H.; Li, Q.; Graham, M. J.; Greiner, A.; Reneker, D. H.; Harris, F. W.; Cheng, S. Z. D. *J. Am. Chem. Soc.* **2004**, *126*, 15754.

(20) Ding, B.; Kim, H.; Kim, C.; Khil, M.; Park, S. *Nanotechnology* **2003**, *14*, 532.

(21) Li, D.; Ouyang, G.; Xia, Y. *Nano. Lett.* **2005**, *5*, 913.

(22) Zong, X. H.; Ran, S. F.; Kim, K. S.; Fang, D. F.; Hsiao, B. S.; Chu, B. *Biomacromolecules* **2003**, *4*, 416.

(23) Wnek, G. E.; Carr, M. E.; Simpson, D. G.; Bowlin, G. L. *Nano Lett.* **2003**, *3*, 213.

(24) Wang, X. Y.; Drew, C.; Lee, S. H.; Senecal, K. J.; Kumar, J.; Samuelson, L. A. *Nano Lett.* **2002**, *2*, 1273.

(25) Sanders, E. H.; Kloefkorn, R.; Bowlin, G. L.; Simpson, D. G.; Wnek, G. E. *Macromolecules* **2003**, *36*, 3803.

(26) Zeng, J. H.; Su, J.; Li, Z. H.; Yan, R. X.; Li, Y. D. *Adv. Mater.* **2005**, *17*, 2119.

(27) Mai, H. X.; Zhang, Y. W.; Si, R.; Yan, Z. G.; Sun, L. D.; You, L. P.; Yan, C. H. *J. Am. Chem. Soc.* **2006**, *128*, 6426.

(28) Mai, H. X.; Zhang, Y. W; Sun, L. D.; Yan, C. H. *J. Phys. Chem. C* **2007**, *111*, 13721.

(29) Mai, H. X.; Zhang, Y. W; Sun, L. D.; Yan, C. H. *J. Phys. Chem. C* **2007**, *111*, 13730.

(30) Aebischer, A.; Hostettler, M.; Hauser, J.; Krämer, K.; Weber, T.; Güdel, H. U.; Bürgi, H.-B. *Angew. Chem., Int. Ed.* **2006**, *45*, 2802.

(31) Auzel, F. *Chem. Rev.* **2004**, *104*, 139.

(32) Krämer, K. W.; Biner, D.; Frei, G.; Güdel, H. U.; Hehlen, M. P.; Lüthi, S. R. *Chem. Mater.* **2004**, *16*, 1244.

(33) Suyver, J. F.; Grim, J.; Güdel, H. U. *J. Lumin.* **2005**, *114*, 53.

(34) Heer, S.; Kömpe, K.; Güdel, H. U.; Haase, M. *Adv. Mater.* **2005**, *16*, 2102.

(35) Yu, H.; Song, H.; Pan, G.; Li, S.; Liu, Z.; Bai, X.; Wang, T.; Lu, S.; Zhao, H. *J. Lumin.* **2007**, *124*, 39.

(36) Bai, X.; Song, H.; Pan, G.; Lei, Y.; Wang, T.; Ren, X.; Lu, S.; Dong, B.; Dai, Q.; Fan, L. *J. Phys. Chem. C* **2007**, *111*, 13611.

(37) Thrash, R. J.; Johnson, L. F. *J. Opt. Soc. Am. B* **1994**, *11*, 881.

(38) Auzel, F. *C. R. Acad. Sci. Paris* **1966**, *263b*, 819.

(39) Sivakumar, S.; van Veggel, F. C. J. M.; Raudsepp, M. *J. Am. Chem. Soc.* **2005**, *127*, 12464.